The Journal of Chemical Physics

Design of nearly perfect hyperuniform polymeric materials

Cite as: J. Chem. Phys. **153**, 054902 (2020); https://doi.org/10.1063/5.0017861
Submitted: 10 June 2020 . Accepted: 15 July 2020 . Published Online: 05 August 2020

Alexandros Chremos

The Journal of Chemical Physics ARTICLE scitation.org/journal/jcp

Design of nearly perfect hyperuniform polymeric materials

Cite as: J. Chem. Phys. 153, 054902 (2020); doi: 10.1063/5.0017861
Submitted: 10 June 2020 • Accepted: 15 July 2020 •
Published Online: 5 August 2020

Alexandros Chremos[a)]

AFFILIATIONS

Section on Quantitative Imaging and Tissue Sciences, Eunice Kennedy Shriver National Institute of Child Health and Human Development, National Institutes of Health, Bethesda, Maryland 20892, USA

[a)]Author to whom correspondence should be addressed: alexandros.chremos@nih.gov

ABSTRACT

Disordered hyperuniform materials are exotic amorphous systems that simultaneously exhibit anomalous suppression of long-range density fluctuations, comparable in amplitude to that of crystals and quasi-crystalline materials, while lacking the translational order characteristic of simple liquids. We establish a framework to quantitatively predict the emergence of hyperuniformity in polymeric materials by considering the distribution of localized polymer subregions, instead of considering the whole material. We demonstrate that this highly tunable approach results in arbitrarily small long-range density fluctuations in the liquid state. Our simulations also indicate that long-ranged density fluctuation of the whole polymeric material is remarkably insensitive to molecular topology (linear chain, unknotted ring, star, and bottlebrush) and depends on temperature in an apparently near universal fashion. Our findings open the way for the creation of nearly perfect hyperuniform polymeric materials.

https://doi.org/10.1063/5.0017861

I. INTRODUCTION

The lossless propagation of electromagnetic or sound waves in a material requires the lack of structural heterogeneities in the material that induce wave scattering. Perfect crystals and quasicrystals belong to this class of materials since their atoms are distributed in space so that the long-ranged density fluctuations are completely suppressed, an effect that can be directly observed in x-ray, light, or neutron scattering experiments. This special class of materials is called hyperuniform.[1,2] However, crystals are not the only materials that are hyperuniform. *Disordered* and *isotropic* materials that exhibit hyperuniformity are attracting attention[1–6] for potential use for a wide range of applications, including biological tissue,[7] photonic band gap materials,[8–10] 2D-materials,[11] enhanced pinning in superconductors,[12] terahertz quantum lasing,[13] as well as enhancement of optical[14] and mechanical properties.[15,16] There are two key advantages for these materials over crystals, the high defect tolerance[17] and isotropy, which are necessary for the creation of isotropic thermal radiation sources[18] and waveguides with an arbitrary bending angle.[19] While disordered hyperuniform patterns have been observed in nature in the distribution of photo-receptors of core cells in avian eyes[7] and limited cases have been reproduced with model systems, such as emulsified droplets[3] and the glassy minority blocks of sphere-forming block copolymers,[4] the practical creation of amorphous hyperuniform materials remains a challenge.

Liquids are typically disordered and isotropic, making them potential candidates for disordered hyperuniform materials. However, they are subject to thermal fluctuations that contribute to the long-range density fluctuations, disrupting hyperuniformity in the liquid state. Indeed, most proposed hyperuniform materials, such as strictly jammed hard spheres[1] and emulsified droplets,[3] operate at thermodynamic conditions or length scales where thermal fluctuations are negligible or in off-equilibrium conditions.[2,20] Thus, the challenge for a liquid to be hyperuniform in equilibrium is that its long-range density fluctuations must be nearly completely suppressed in amplitude as in a crystal while retaining its flow characteristics. This can be understood quantitatively by defining the "degree of hyperuniformity" h as the ratio of the structure factor $S(q)$ in the limit $q \to 0$, related to long-ranged density fluctuations, over the value of $S(q)$ at the first peak S_p, which represents the degree of particle localization at the average interparticle

distance.[2,17] Correspondingly, $h = 0$ for a perfect hyperuniform material, but more generally, a material at equilibrium is considered "effectively hyperuniform" if h satisfies the inequality $h \equiv S(0)/S_p < 10^{-3} \equiv h_0$.[2,17] Typical simple liquids exhibit $h \approx 10^{-2}$, while h in amorphous ice progressively approaches h_0 at elevated pressures and low temperatures.[21] Models of superfluid 4He[22] and one-component plasma[23] have been suggested to be hyperuniform.[2] However, no material suitable for manufacturing has been reported to exhibit $h \ll h_0$.

Polymer melts above the glass transition temperature T_g behave similar to simple liquids, and they exhibit $h \gtrsim h_0$ in the liquid state even near T_g.[24] We have showed recently that the degree of hyperuniformity of the distribution of localized substituent parts (e.g., backbone in bottlebrushes) of the polymer, h_L, exhibits enhanced hyperuniformity, $h_L < h_0$,[25,26] but there is little understanding on how h and h_L are related. Moreover, a direct calculation of h_L requires expensive large scale simulations that need to be repeated for each molecular structure and thermodynamic state. In our investigation, we expand upon our previous phenomenological observations by establishing a material design framework to quantitatively predict the emergence of hyperuniformity in polymer melts at equilibrium, evaluated over a wide range of molecular structures, molecular masses, and temperatures. Our proposed framework provides an understanding of how molecular characteristics influence h_L, and it significantly reduces the cost in the estimation of h_L. Moreover, it provides material design pathways for the practical creation of polymeric materials that exhibit *nearly perfect* hyperuniformity, $h_0 \gg h_L \to 0$, even in the liquid state.

II. MODEL AND METHODS

Our system consists of N_p polymers, ranging from $N_p = 400$ to 250 000 polymers. A bottlebrush polymer is composed by a linear chain having N_b segments as the backbone and side chains of M segments each. Each bottlebrush polymer has f side chains, where one of their free ends is grafted along the backbone chain in a uniform fashion. Thus, the total number of interaction centers per bottlebrush polymer is $M_w = fM + N_b$. A star polymer is effectively a bottlebrush having the shortest possible backbone, i.e., $N_b = 1$. Thus, the backbone becomes the core particle at which f side chains are grafted on its surface. A linear chain is a special case of star polymers, and by extension of bottlebrushes, from the bottlebrush model, one recovers the linear chain molecular architecture by having $N_b = 1$ (as in star polymers) and $f = 2$. The main focus of the current study is on the following molecular architectures: linear chains ($f = 2$ arms) having $M = 5$ and $M = 40$ segments per arm, star polymers having $f = 8$, 16 arms and $M = 5$ segments, and bottlebrush polymers having $N_b = 40$ backbone segments, $f = 40$ side chains, and $M = 10$ segments per side chain. A schematic illustrating the key features of different molecular architectures is presented in Fig. 1(a). The interactions between all types of segments are described by the cut-and-shifted Lennard-Jones (LJ) potential, where ε and σ define the units of energy and length, and a cutoff distance $r_c = 2.5\sigma$. Additionally, segments along a chain are connected via a stiff harmonic spring, $V_H(r) = k(r - l_0)^2$, where $l_0 = 0.99\sigma$ is the equilibrium length of the spring and $k = 2500\varepsilon/\sigma^2$ is the spring constant. In terms of the units of real polymer chains, the beads should be identified with statistical segments of flexible polymer having a typical scale of 1 nm–2 nm.

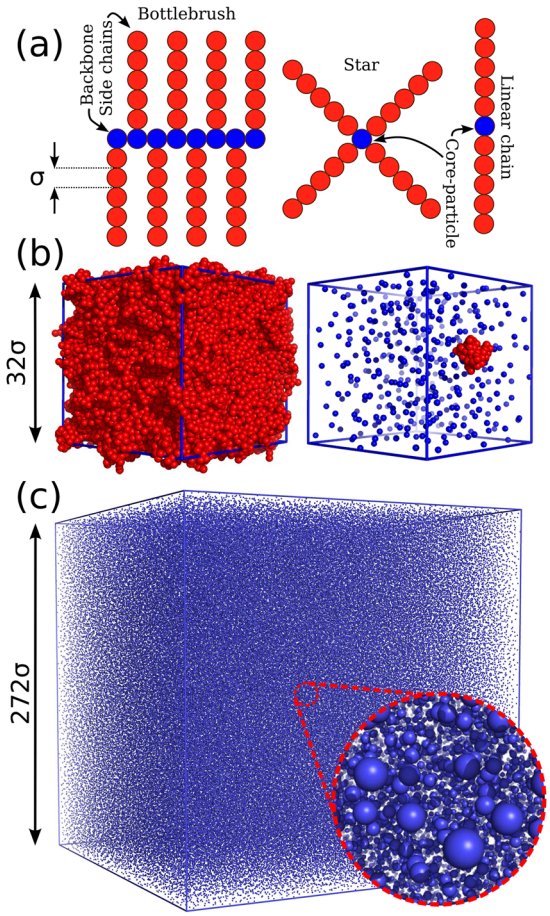

FIG. 1. (a) Schematic illustration of the topological architecture of linear chain, regular star, and bottlebrush polymers. (b) Screenshots of a polymer melt composed of 400 stars, having $f = 16$ arms and $M = 5$ arm length, with all the segments visible (left) and only the core particles along with a single star are visible for visualization purposes (right). (c) Screenshot of the core particles of a polymer melt composed of 250 000 star polymers, the same type as in (b), corresponding to 20 250 000 interaction centers; these large scale simulations were necessary to probe hyperuniformity.

Simulations were performed in a cubic box with length L; periodic boundary conditions were applied in all three directions. We utilized the large-scale atomic/molecular massively parallel simulator (LAMMPS).[31] Simulations were performed in the NVT ensemble after equilibration in the NPT ensemble at the desired temperature. Time averaging was conducted for $O(10^8)$ time steps after equilibration. The time step was set to $\delta t = 0.005\tau$, where $\tau = \sigma(m/\varepsilon)^{1/2}$ is the unit of time, where m is the unit of mass and it is set $m = 1$ for the purposes of our study. Temperature and pressure are measured in units of ε/k_B and σ^3/ε, respectively. Simulations were performed at different temperatures and $\langle P \rangle \approx 0.1$ in reduced units.

III. RESULTS AND DISCUSSION

Our focus is on understanding how enhanced hyperuniformity emerges in polymer melts. We will briefly discuss that polymer melts as a whole is not hyperuniform due to thermal fluctuation present in the liquid state. Specifically, the segmental packing as a function of T and P for different molecular architectures and molecular masses results in all cases $h \gtrsim h_0$. Subsequently, we discuss the degree of hyperuniformity of the distribution of localized parts of the polymer structure h_L, and we will discuss the challenges involving the direct calculation of h_L. Specifically, the packing of the localized substituent parts of the polymer structure is on length scales comparable to the size of the whole polymer, which can be several orders of magnitude larger than the length scales related to segmental packing, thus requiring prohibitively expensive simulations to probe the long-ranged density fluctuations of the localized substituent parts of the polymer structure. We will also propose and evaluate a set of relations that predict h_L for different molecular architectures, molecular masses, and thermodynamic conditions in the liquid state, thus resolving the challenge of calculating h_L.

A. Thermodynamics of polymer liquids

For liquids in equilibrium, it is well known that the structure factor at zero-wave-vector, $S(q \to 0)$ is related to segmental density ρ and isothermal compressibility κ_T as[32]

$$S(0) = \rho\, k_B T\, \kappa_T, \tag{1}$$

where k_B is the Boltzmann constant. If ρ and κ_T can be determined with a direct calculation or via an established correlation function, see the supplementary material, then $S(0)$ can be easily determined. Alternatively, $S(0)$ can be directly obtained by the plateau formed in $S(q)$ at $q\,\sigma < 1$, where σ is the unit of length and the size of a polymer segment (see Fig. 1). We note that $S(q)$, and by extension $S(0)$, is determined by considering the contribution of all the polymer segments in the polymer melt. Examples of the polymer melts are presented in Fig. 1. We proceed by briefly summarizing the trends of ρ and κ_T in polymer liquids.

For polymer chains, it is known that ρ follows the Fox–Flory relationship, $\rho_\infty - \rho \sim 1/M_w$, where the density of the polymer melt reaches to a plateau, ρ_∞, for long polymer chains approximately above the entanglement threshold.[33,34] For branched polymers, ρ also follows the general behavior, as described by the Fox–Flory relationship, but with some important differences. First, branching, as in the cases of star and bottlebrush polymers, forms more dense systems compared to linear chain melts. Specifically, for highly branched star polymers, ρ *decreases* with an increase in M_w, which is the opposite trend occurring in linear chain systems. Star polymers having a moderate number of arms ($f \approx 5$ to 6 arms) are found to be at the crossover between these two extremes.[28,29] At this crossover, other notable polymer architectures are also found, such as bottlebrush[30] and unknotted ring polymers.[29] Analogous M_w and molecular architecture effects are found for κ_T, where highly branched polymers are less compressible compared to linear polymer chains.[30] As $M_w \to \infty$, the effect of molecular architecture on ρ and κ_T becomes diminished[28–30] [see Fig. 2(a)].

To assess the influence of molecular topology and M_w on hyperuniformity, we need to estimate $S(0)$, which might vanish for a combination of polymer topology and M_w. Surprisingly, we find that all different molecular architectures considered, irrespective of whether the polymers are entangled or not, have nearly the same $S(0)$ at a given temperature and pressure [Fig. 2(b)]. The results for $S(0)$ suggest that the molecular architecture has little influence

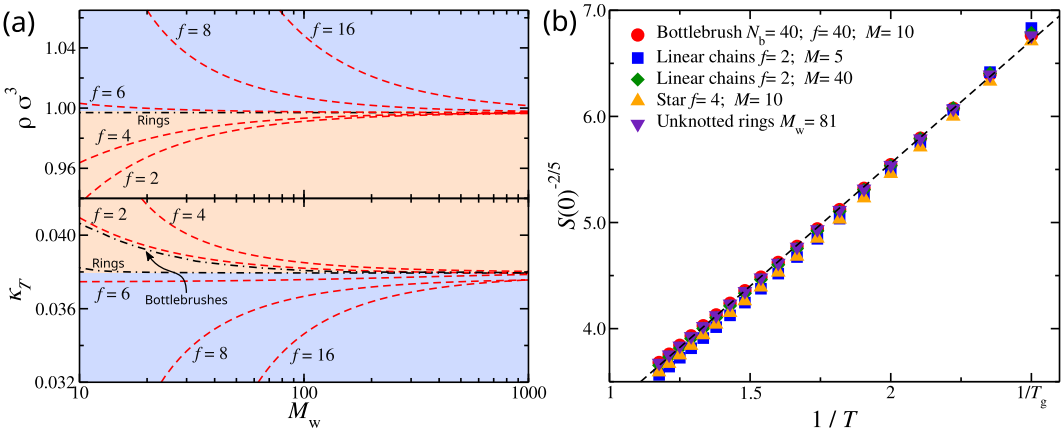

FIG. 2. (a) Segmental density ρ and isothermal compressibility κ_T at temperature $T = 0.5$ as a function of the molecular mass, M_w. Dashed lines correspond to segmental correlations based on Dobkowski's correlation function[27] for linear chain and star polymers. The dotted-dashed lines represent ρ and κ_T of unknotted ring and bottlebrush polymers. For more information on the results for star and ring polymers, see Refs. 28 and 29, and for bottlebrush polymers, see Ref. 30. The highlighted regions correspond to polymers having (pale orange) highly anisotropic linear chain-like conformations and (blue) highly symmetric particle-like conformations. (b) Total structure factor $S(q)$ of polymers at zero-wave-vector ($q = 0$) obtained from Eq. (1) as a function of $1/T$. Details on the results can be found in the supplementary material and Ref. 30. The dashed line, $S(0)^{-2/5} = 2.31/T + 0.93$, is a guide for the eye. The glass transition temperature is $T_g \approx 0.4$.[28,29]

on the segmental long-scale density fluctuations because the segments fill the space in relatively the same way as $q \to 0$ though "residues" of thermal fluctuations keep $S(0)$ non-zero. Since $S(0)$ is approximately the same, then the molecular architecture influences ρ and κ_T so that $1/\rho \sim \kappa_T$, more dense polymeric materials are less compressible.

Furthermore, we find that $S(0)$ can be described by the simple relationship,

$$S(0)^{-2/5} = \frac{\alpha}{T} + \beta, \tag{2}$$

where α and β describe the "enthalpic" and "entropic" contributions, respectively; α and β are pressure dependent. This empirical relation has the same functional form of a typical energy parameter in a polymer fluid, e.g., Flory–Huggins χ-parameter.[35] A similar relation has been derived by Schweizer and Saltzman,[36] where the exponent for $S(0)$ was $-1/2$, and evaluated with experimental data for linear polymer chains. However, we are not aware of any theoretical derivation of the relation with exponent $-2/5$. In our polymer model at low temperatures, $S(0)$ can be described by a power law relation with an exponent of $-1/2$, but the errors are larger (not shown here). Nevertheless, this disagreement signifies that these relations need to be tested over an even wider temperature range. We find Eq. (2) to agree well for all polymer architectures investigated in our study for a temperature range $1 \lesssim T/T_g \lesssim 3$.

Equation (2) provides insight into the packing efficiency of polymer segments in polymer melts at equilibrium. As T decreases toward $T_g \approx 0.4$,[28,29] the density fluctuations are progressively suppressed, resulting in $S(0) \approx 0.009$ at T_g. The value of $S(q)$ at its first peak, S_p, also changes with T variation and increases in the case of linear chains as $S_p \approx 0.68 + 1.38/T$. For the sake of the argument, we assume that the segmental localization characterized by S_p is similar between the different molecular architectures. This leads to $S_p \approx 4.13$ at T_g and $h \approx 0.002 > h_0$, meaning the polymer melt progressively approaches hyperuniformity, but h is not sufficiently small enough to be considered effectively hyperuniform. If we assume that Eq. (2) holds for $T < T_g$, then the temperature at which the segmental long-range density fluctuations are suppressed sufficiently for $h = h_0$ is $T_h \approx 0.31$, which is well below T_g.

B. Design hyperuniform polymeric material

While the whole polymer melt does not exhibit enhanced hyperuniformity, it does not prevent the design of a material with this feature. We have demonstrated previously that the structure factor of the *localized* polymer subregions, $S_L(q)$, exhibits appreciable suppression of the long-ranged density fluctuations such that $h_0 > h_L$.[25,26] The focus on a subset of the polymer structure provides significant practical advantages since the selected segments can be functionalized to exhibit dielectric or mechanical properties that distinguish them from the rest of the material and have observable consequences. For example, the backbone of bottlebrush polymers can be composed of conductive polymers,[37,38] and the nanoparticles can be metallic, semiconducting, magnetic, etc.,[39,40] in the case of star-like polymer-grafted nanoparticles. However, there are two missing components for establishing a design framework of hyperuniform polymeric materials: (i) reducing the cost of $S_L(0)$ estimation, and by extension h_L, since expensive large scale simulations for each molecular structure and thermodynamic state are required, (ii) an understanding on how molecular characteristics influence h_L.

We expand upon previous phenomenological observations[25,26] and establish the foundations of a design framework for hyperuniform polymeric materials. Specifically, we propose an equation that provides a remarkably simple prediction for $S_L(0)$ (see the supplementary material for its derivation),

$$S_L(0) = \frac{M_L}{M_w} S(0), \tag{3}$$

where M_L is the molecular mass of the subset of polymer segments that composed the localized polymer subregion. Previously, we identified examples of "localized" polymer subregions as the core of the stars and polymer-grafted nanoparticles and the backbone of bottlebrush polymers.[25,26] Here, the degree of localization of polymer segments is determined by the segmental relaxation at length scales comparable to the polymer size, i.e., higher relaxation time corresponds to higher degree of localization. For example, the most localized polymer segment in star polymers is the core particle, while the rest of the segments have lower relaxation times depending on their distance from the core particle due to the intra-molecular heterogeneity of star polymers[28] (see Fig. 3). Equation (3) can be applied for different subsets of localized polymer segments so long they are chosen symmetrically from the most localized segment in the polymer structure. The concept that a subset of polymer segments in the melt exhibits suppressed long-ranged correlations is counter-intuitive since parts of the material are left out in the calculation, effectively creating voids. Our findings suggest that the packing of the localized substituent parts of the polymers is different than the rest of the polymer structure.

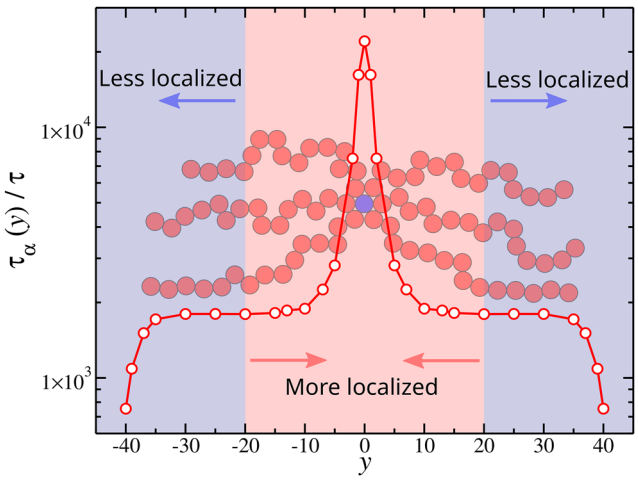

FIG. 3. Structural relaxation time, τ_α, along a grafted chain for a star polymer having $f = 12$ arms and $M = 40$ as a function of the index of the segment along the arm y with $y = 0$ and $y = M$ being the core particle and the free-end, respectively; for more information, see Ref. 28. The behavior of τ_α at $y < 0$ is a reflection of $y > 0$, and the highlighted regions and arrows outline the regions of which segments are more or less localized.

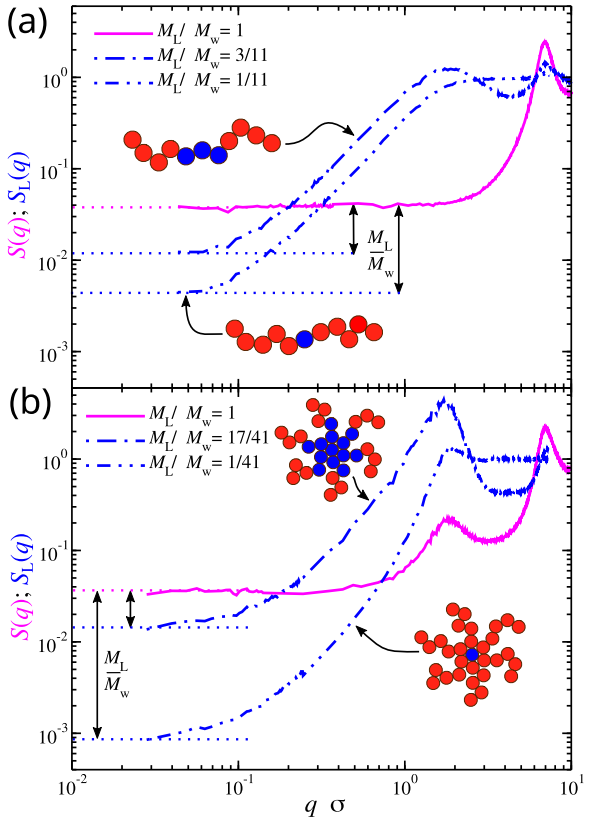

FIG. 4. Total static structure factor $S(q)$ (magenta) and the structure factor $S_L(q)$ of the localized polymer subregions having molecular mass M_L (blue) are presented for different molecular architectures: (a) linear chains having molecular mass M_w = 11 and (b) star polymers having f = 8 arms and M_w = 41. The magenta dotted lines correspond to the fit of the plateau of $S(q)$ in the low q regime.

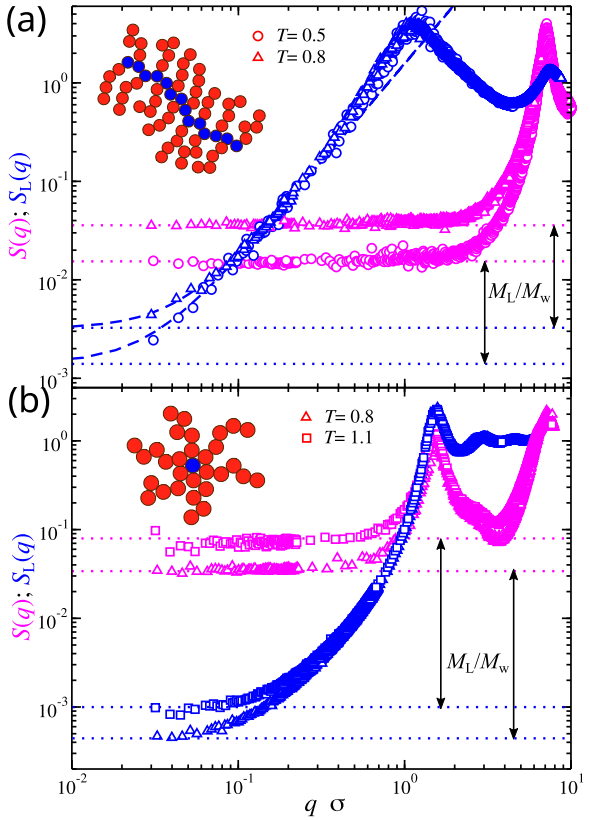

FIG. 5. Total static structure factor $S(q)$ (magenta) and the structure factor $S_L(q)$ of the localized polymer subregions having molecular mass M_L (blue) are presented for different molecular architectures: (a) bottlebrush polymers having a backbone molecular mass N_b = 40, f = 40 side chains, M = 10 segments per side chain, and total molecular mass M_w = 440 and (b) star polymers having f = 16 arms and M_w = 81. The magenta dotted lines correspond to fit of the plateau of $S(q)$ in the low q regime, while the blue dotted lines are the result of the fits for $S(0)$ divided by M_L/M_w. The dashed lines in (a) correspond to fits based on a power–law relation: $S_L(q) = S_0(1 + cq^2)$, where c and S_0 are fitting parameters.

We validate Eq. (3) over different polymer architectures, a wide range of temperatures, and ratios of M_L/M_w by taking the following steps. We determined the plateau in $S(q)$ at the $q\sigma < 1$ region to obtain $S(0)$ for different molecular architectures and temperatures. The values of $S(0)$ were in agreement with the predictions from empirical correlations such as Eq. (1) (see also the supplementary material), suggesting that our systems are in equilibrium.[41] In a similar fashion, $S_L(0)$ was obtained either by determining the height of the plateau formed as $q \to 0$ in the case of linear chains and star polymers, as seen in Figs. 4 and 5(b), or by extrapolation by fitting $S_L(q)$ to the relation $S_L(q) = S_0(1 + cq^2)$ for bottlebrush polymers, where c and S_0 are fitting parameters [see Fig. 5(a)]. The ratio $S_L(0)/S(0)$ obtained from calculations of $S(q)$ and $S_L(0)$ is approximately equal to M_L/M_w for all cases examined, as seen in Figs. 4 and 5, which is in excellent agreement with the prediction of Eq. (3).

We also considered the validity of Eq. (3) when the interactions between localized segments are different from the rest of the material. If the strength of these interactions, ε_c, is strong enough, say in the case of linear chains, then the localized segments will cluster forming assemblies that resemble star-like polymers. Thus, it is not surprising that the resulting $S_L(q)$ curves resemble the curves from regular star polymers [compare Figs. 4(b) and 6]. We also find Eq. (3) to be valid for different strength of these attractive interactions, suggesting that one can view different molecular architectures as the result of more complex interactions between different parts of the polymer structure, e.g., if the resulting clusters were highly anisotropic, then the central segments would form assemblies that would resemble bottlebrushes. The demonstration of the applicability of Eq. (3) for different molecular structures, molecular masses, temperatures, and different interactions reflects the generality and robustness of our proposed relation.

The significance of Eq. (3) is that h_L can be obtained without performing expensive large scale simulations needed for the calculation of $S_L(0)$,

$$h_L \equiv \frac{S_L(0)}{S_{p,L}} = \frac{M_L}{M_w}\frac{S(0)}{S_{p,L}}, \tag{4}$$

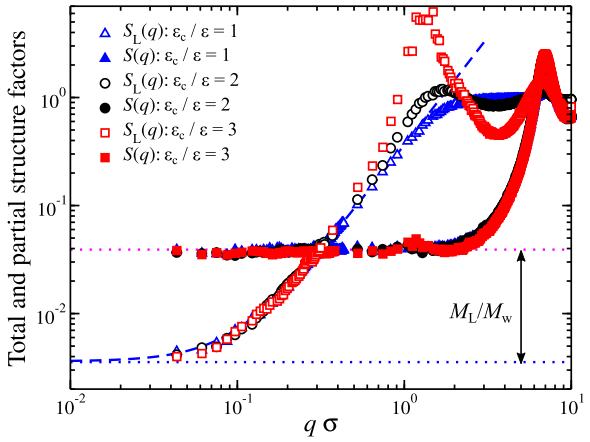

FIG. 6. Total and partial structure factors of linear polymer chains, having $M_w = 11$ and $M_L = 1$, at different strengths of interaction $\varepsilon_c/\varepsilon = 1$, 2, and 3 between the core–core segments and $T = 0.8$. The magenta dotted lines correspond to the fit of the plateau of $S(q)$ in the low q regime, while the blue dotted lines are the result of the fits for $S(0)$ divided by M_L/M_w. The dashed line corresponds to fits based on a power-law relation: $S_L(q) = S_0(1 + cq^2)$, where c and S_0 are fitting parameters.

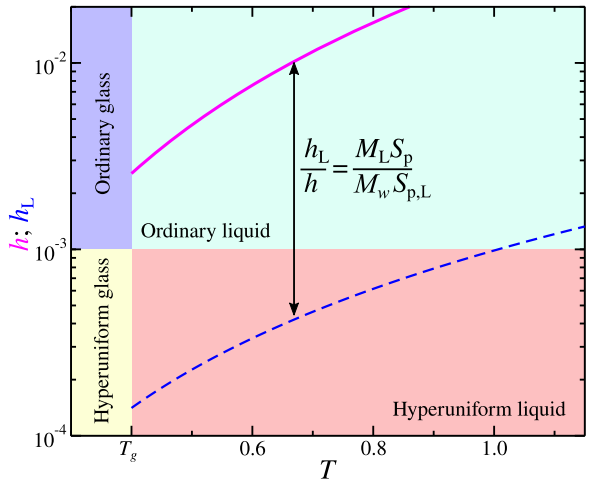

FIG. 7. Schematic for the degree of hyperuniformity h (continuous line) of the polymer melt as a whole and the localized polymer subregion h_L (dashed line) [see also Eq. (6)].

where $S_{p,L}$ is the value of $S_L(q)$ at the position of the first peak. It is evident from Fig. 5(a) that the length scale needed to obtain $S_L(0)$ without fitting is $q\,\sigma \approx 6 \times 10^{-3}$, which corresponds to over 10^9 interaction centers making the simulations prohibitively expensive; larger polymer structures require a even larger length scale for $S_L(q \to 0)$ reaching a plateau. However, the terms in the right-hand side of Eq. (4) can be obtained in the high q regime, i.e., smaller length scales. Based on our example, S_L and $S(0)$ to be reliably estimated require simulations having a system size of $q\sigma \approx 3 \times 10^{-1}$ corresponding to 9×10^4 interaction centers. This is four orders of magnitude smaller than if we had to calculate $S_L(0)$ directly; thus, Eq. (4) accelerates the material design process of hyperuniform polymeric materials.

Two material design rules can be formalized on how to suppress long-range density fluctuations of the polymer subregions. First, $S_L(0)$ has the same temperature dependence as with $S(0)$, which scales as $S(0) \sim T^{-5/2}$ according to Eq. (2). This is expected since annealing a material typically leads to appreciated compression of density fluctuations. The scaling of h_L can be obtained from Eqs. (2) and (4) so that

$$h_L = \frac{M_L}{M_w}\frac{1}{S_{p,L}}\left(\frac{\alpha}{T} + \beta\right)^{-5/2}. \tag{5}$$

This design rule is consistent with the idea that hyperuniformity emerges in jammed systems based on a conjecture on the jamming of hard spheres[1] and evaluated by simulations[42] and experiments.[43] Second, $S_L(0) \sim M_L/M_w$, meaning that h_L decreases as M_L/M_w becomes smaller. This is important because $h \gtrsim h_0$ for $T \gtrsim T_g$, and thus, a ratio of $M_L/M_w \ll 1$ can greatly reduce h_L well below h_0, even at temperatures well above T_g (see Fig. 7). In other words, Eq. (3) provides a design pathway for the creation of *nearly perfect hyperuniform* polymeric materials at any temperature in the liquid state since $S_L(0) \to 0$, and by extension $h_L \to 0$, as $M_w \to \infty$ and M_L remains finite. Unlike the first design rule, the second one shows that jamming is not essential for the emergence of hyperuniformity.

Another consequence is that Eq. (3) is agnostic to the type of the molecular architecture of the polymer. This means that any one-component polymer fluid can be designed so that the distribution of the localized subregions of the polymer structure exhibit enhanced hyperuniformity, $h_L \ll h_0$. However, the choice of molecular architecture is still important, and it is better understood if we rewrite Eq. (4) as follows:

$$\frac{h_L}{h} = \frac{M_L}{M_w}\frac{S_p}{S_{p,L}}. \tag{6}$$

A decrease in h_L can be achieved by enhancing the degree of localization in the substituent parts of the polymer structure with respect to the rest of the material, i.e., decreasing the value of $S_p/S_{p,L}$ (Fig. 7); note that $h \approx h_0$ near T_g in polymer liquids.[24,26] Branching enhances the degree of localization of the polymer parts at and near the branching points [compare Fig. 4(a) with Figs. 4(b) and 5], confirming our previous phenomenological observation that hyperuniform configuration of particles can be achieved by "dressing" the particle or molecule of interest by a polymeric layer;[26] typical values of $S_{p,L}$ are in the range of $1 \lesssim S_{p,L} \lesssim 8$ (see Figs. 4 and 5). Branching also reduces the effect of entanglements.[44,45] Indeed, linear chains (no branching), having large molecular weight, are slow to reach equilibrium due to the rise of entanglements and may become an issue in practice; entanglements start to emerge in our model at $M_w \approx 85$.[46] Thus, highly branched molecular architectures are promising candidates because they provide a wider range of molecular masses that can be utilized for the practical creation of hyperuniform polymeric materials.

Finally, it is important to emphasize that while the localized polymer subregions exhibit enhanced hyperuniformity, the polymer melt has liquid-like flow characteristics since $T > T_g$. In other words, the long-range density fluctuations for the localized polymer subregions can be hyperuniform despite the polymer mobility, suggesting the existence of highly cooperative motions at scales larger than the polymer size so that hyperuniformity is preserved in the liquid state. Indeed, in the case of one-component fluids composed of polymer-grafted nanoparticles (similar to star polymer melts), where the distribution of the nanoparticles exhibit hyperuniform features, we previously found that the nanoparticles become superdiffusive by thermal annealing,[25] a feature observed experimentally.[47] Our proposed set of equations provide a framework to design materials that exhibit novel dynamics.

IV. CONCLUSIONS

In summary, we used molecular dynamics simulations to establish a material design framework for the practical creation of nearly perfect hyperuniform polymeric materials by quantitatively predicting the degree of hyperuniformity for the polymeric material and the localized substituent parts in the polymer as characterized by h and h_L, respectively. We demonstrate that while there is a limit in suppressing the long-ranged density fluctuations, $S(q \to 0)$, associated with the thermal fluctuations as the polymer melt approaches the glass transition temperature T_g similar to the limit found in other simple liquids, the long-range density fluctuations of the localized subregion of the polymers (e.g., the cores of the stars or backbone chains of the bottlebrush molecules), as characterized by $S_L(0)$, is related to $S(q \to 0)$ and the ratio of molecular mass of the localized part of the polymer over the polymer molecular mass, M_L/M_w. This simple relation provides two significant benefits: (i) estimation of $S_L(0)$ can be determined by quantities obtained at orders of magnitude smaller length scales than in the case of directly calculating $S_L(0)$, thus accelerating the pace of the material design process and (ii) one can tune M_L/M_w by redesigning the molecular structure to make $S_L(0)$, and by extension h_L, vanishing small and comparable in amplitude to that of crystals and quasi-crystalline materials even at temperatures well above T_g. In other words, polymer liquids can be designed to exhibit material properties, associated with long-ranged density fluctuations, at the same efficiency as with crystalline materials. Our material design framework—evaluated over a wide range of molecular structures (linear chains, stars, and bottlebrushes), molecular masses, and temperatures—opens venues for the creation of *nearly perfect* hyperuniform polymeric materials.

SUPPLEMENTARY MATERIAL

See the supplementary material for additional information on thermodynamic quantities of polymer melts.

ACKNOWLEDGMENTS

A.C. is thankful for insightful discussions with Jack F. Douglas and Salvatore Torquato.

DATA AVAILABILITY

The data that support the findings of this study are available from the corresponding author upon reasonable request.

REFERENCES

[1] S. Torquato and F. H. Stillinger, "Local density fluctuations, hyperuniformity, and order metrics," Phys. Rev. E **68**, 041113 (2003).
[2] S. Torquato, "Hyperuniform states of matter," Phys. Rep. **745**, 1–95 (2018).
[3] J. H. Weijs, R. Jeanneret, R. Dreyfus, and D. Bartolo, "Emergent hyperuniformity in periodically driven emulsions," Phys. Rev. Lett. **115**, 108301 (2015).
[4] G. Zito, G. Rusciano, G. Pesce, A. Malafronte, R. Di Girolamo, G. Ausanio, A. Vecchione, and A. Sasso, "Nanoscale engineering of two-dimensional disordered hyperuniform block-copolymer assemblies," Phys. Rev. E **92**, 050601 (2015).
[5] J. Kim and S. Torquato, "Methodology to construct large realizations of perfectly hyperuniform disordered packings," Phys. Rev. E **99**, 052141 (2019).
[6] M. A. Klatt, J. Lovrić, D. Chen, S. C. Kapfer, F. M. Schaller, P. W. Schönhöfer, B. S. Gardiner, A. S. Smith, G. E. Schröder-Turk, and S. Torquato, "Universal hidden order in amorphous cellular geometries," Nat. Commun. **10**, 811 (2019).
[7] Y. Jiao, T. Lau, H. Hatzikirou, M. Meyer-Hermann, J. C. Corbo, and S. Torquato, "Avian photoreceptor patterns represent a disordered hyperuniform solution to a multiscale packing problem," Phys. Rev. E **89**, 022721 (2014).
[8] M. Florescu, P. J. Steinhardt, and S. Torquato, "Optical cavities and waveguides in hyperuniform disordered photonic solids," Phys. Rev. B **87**, 165116 (2013).
[9] L. S. Froufe-Pèrez, M. Engel, P. F. Damasceno, N. Müller, J. Haberko, S. C. Glotzer, and F. Scheffold, "Role of short-range order and hyperuniformity in the formation of band gaps in disordered photonic materials," Phys. Rev. Lett. **117**, 053902 (2016).
[10] S. R. Sellers, W. Man, S. Sahba, and M. Florescu, "Local self-uniformity in photonic networks," Nat. Commun. **8**, 14439 (2017).
[11] Y. A. Gerasimenko, I. Vaskivskyi, M. Litskevich, J. Ravnik, J. Vodeb, M. Diego, V. Kabanov, and D. Mihailovic, "Quantum jamming transition to a correlated electron glass in 1T-TaS_2," Nat. Mater. **18**, 1078–1083 (2019).
[12] Q. Le Thien, D. McDermott, C. J. O. Reichhardt, and C. Reichhardt, "Enhanced pinning for vortices in hyperuniform pinning arrays and emergent hyperuniform vortex configurations with quenched disorder," Phys. Rev. B **96**, 094516 (2017).
[13] R. Degl'Innocenti, Y. D. Shah, L. Masini, A. Ronzani, A. Pitanti, Y. Ren, D. S. Jessop, A. Tredicucci, H. E. Beere, and D. A. Ritchie, "Hyperuniform disordered terahertz quantum cascade laser," Sci. Rep. **6**, 19325 (2016).
[14] O. Leseur, R. Pierrat, and R. Carminati, "High-density hyperuniform materials can be transparent," Optica **3**, 763–767 (2016).
[15] Y. Xu, S. Chen, P.-E. Chen, W. Xu, and Y. Jiao, "Microstructure and mechanical properties of hyperuniform heterogeneous materials," Phys. Rev. E **96**, 043301 (2017).
[16] S. Torquato and D. Chen, "Multifunctional hyperuniform cellular networks: Optimality, anisotropy and disorder," Multifunct. Mater. **1**, 015001 (2018).
[17] J. Kim and S. Torquato, "Effect of imperfections on the hyperuniformity of many-body systems," Phys. Rev. B **97**, 054105 (2018).
[18] M. Florescu, K. Busch, and J. P. Dowling, "Thermal radiation in photonic crystals," Phys. Rev. B **75**, 201101 (2007).
[19] H. Miyazaki, M. Hase, H. T. Miyazaki, Y. Kurokawa, and Y. Shynya, "Photonic material for designing arbitrarily shaped waveguides in two dimensions," Phys. Rev. B **67**, 235109 (2003).
[20] J. Wang, J. M. Schwarz, and J. D. Paulsen, "Hyperuniformity with no fine tuning in sheared sedimenting suspensions," Nat. Commun. **9**, 2836 (2018).
[21] F. Martelli, S. Torquato, N. Giovambattista, and R. Car, "Large-scale structure and hyperuniformity of amorphous ices," Phys. Rev. Lett. **119**, 136002 (2017).
[22] L. Reatto and G. V. Chester, "Phonons and the properties of a bose system," Phys. Rev. **155**, 88–100 (1967).
[23] M. Baus and J.-P. Hansen, "Statistical mechanics of simple Coulomb systems," Phys. Rep. **59**, 1–94 (1980).

[24]W.-S. Xu, J. F. Douglas, and K. F. Freed, "Influence of cohesive energy on the thermodynamic properties of a model glass-forming polymer melt," Macromolecules **49**, 8341–8354 (2016).
[25]A. Chremos and J. F. Douglas, "Particle localization and hyperuniformity of polymer-grafted nanoparticle materials," Ann. Phys. **529**, 1600342 (2017).
[26]A. Chremos and J. F. Douglas, "Hidden hyperuniformity in soft polymeric materials," Phys. Rev. Lett. **121**, 258002 (2018).
[27]Z. Dobkowski, "Influence of molecular weight distribution and long chain branching on the glass transition temperature of polycarbonate," Eur. Polym. J. **18**, 563–567 (1982).
[28]A. Chremos, E. Glynos, and P. F. Green, "Structure and dynamical intramolecular heterogeneity of star polymer melts above glass transition temperature," J. Chem. Phys. **142**, 044901 (2015).
[29]A. Chremos and J. F. Douglas, "Communication: When does a branched polymer become a particle?," J. Chem. Phys. **143**, 111104 (2015).
[30]A. Chremos and J. F. Douglas, "A comparative study of thermodynamic, conformational, and structural properties of bottlebrush with star and ring polymer melts," J. Chem. Phys. **149**, 044904 (2018).
[31]S. Plimpton, "Fast parallel algorithms for short-range molecular dynamics," J. Comput. Phys. **117**, 1–19 (1995).
[32]J.-P. Hansen and I. R. McDonald, *Theory of Simple Liquids* (Academic Press, Cambridge, 2006).
[33]T. G. Fox and P. J. Flory, "Second-order transition temperatures and related properties of polystyrene. I. Influence of molecular weight," J. Appl. Phys. **21**, 581–591 (1950).
[34]T. G. Fox and P. J. Flory, "The glass temperature and related properties of polystyrene. Influence of molecular weight," J. Polym. Sci. **14**, 315–319 (1954).
[35]P. J. Flory, *Principles of Polymer Chemistry* (Cornell University Press, Ithaca, 1953).
[36]K. S. Schweizer and E. J. Saltzman, "Theory of dynamic barriers, activated hopping, and the glass transition in polymer melts," J. Chem. Phys. **121**, 1984–2000 (2004).
[37]P. Baek, N. Aydemir, Y. An, E. W. C. Chan, A. Sokolova, A. Nelson, J. P. Mata, D. McGillivray, D. Barker, and J. Travas-Sejdic, "Molecularly engineered intrinsically healable and stretchable conducting polymers," Chem. Mater. **29**, 8850 (2017).
[38]S. E. Root, S. Savagatrup, A. D. Printz, D. Rodriquez, and D. J. Lipomi, "Mechanical properties of organic semiconductors for stretchable, highly flexible, and mechanically robust electronics," Chem. Rev. **117**, 6467–6499 (2017).
[39]N. J. Fernades, H. Koerner, E. P. Giannelis, and R. A. Vaia, "Hairy nanoparticle assemblies as one-component functional polymer nanocomposites: Opportunities and challenges," MRS Commun. **3**, 13–29 (2013).
[40]S. Srivastava, S. Choudhury, A. Agrawal, and L. A. Archer, "Self-suspended polymer grafted nanoparticles," Curr. Opin. Chem. Eng. **16**, 92–101 (2017).
[41]É. Marcotte, F. H. Stillinger, and S. Torquato, "Nonequilibrium static growing length scales in supercooled liquids on approaching the glass transition," J. Chem. Phys. **138**, 12A508 (2013).
[42]A. Donev, F. H. Stillinger, and S. Torquato, "Unexpected density fluctuations in jammed disordered sphere packings," Phys. Rev. Lett. **95**, 090604 (2005).
[43]R. Xie, G. G. Long, S. J. Weigand, S. C. Moss, T. Carvalho, S. Roorda, M. Hejna, S. Torquato, and P. J. Steinhardt, "Hyperuniformity in amorphous silicon based on the measurement of the infinite-wavelength limit of the structure factor," Proc. Natl. Acad. Sci. U. S. A. **110**, 13250–13254 (2013).
[44]S. J. Daslin, M. A. Hillmyer, and F. S. Bates, "Molecular weight dependence of zero-shear viscosity in atactic polypropylene bottlebrush polymers," ACS Macro Lett. **3**, 423–427 (2014).
[45]A. Chremos and J. F. Douglas, "Influence of branching on the configurational and dynamical properties of entangled polymer melts," Polymers **11**, 1045 (2019).
[46]R. S. Hoy, K. Foteinopoulou, and M. Kröger, "Topological analysis of polymeric melts: Chain-length effects and fast-converging estimators for entanglement length," Phys. Rev. E **80**, 031803 (2009).
[47]S. Srivastava, P. Agarwal, R. Mangal, D. L. Koch, S. Narayanan, and L. A. Archer, "Hyperdiffusive dynamics in Newtonian nanoparticle fluids," ACS Macro Lett. **4**, 1149–1153 (2015).